Image reconstruction by aperture diversity blind deconvolution

Mario Ivanov
ECE department, Royal Military College of Canada, Kingston, Canada

Donald McGaughey
ECE department, Royal Military College of Canada, Kingston, Canada

ABSTRACT

A new method of collecting diverse images called aperture diversity is used. The technique involves forming images through different shaped apertures. Incoming wavefronts are collimated and beam-split into two or more paths to ensure the wavefront in each path have the same aberrations. Images are then formed for each path using apertures with different shapes. Since the optical transfer function of the system is an autocorrelation of the generalized pupil function, the transfer functions for each path are different but related, thus giving a strong constraint for minimization. The pupil phase is calculated for each of the channels and sets of simulated images are produced. A combination of two minimizing algorithms is used to obtain the set of Zernike weight estimates the Simplex algorithm and Genetic algorithm. An object independent error metric is minimized to estimate the phase aberrations. The weight estimates are then used to construct object intensity estimates using a Wiener filter. Results from simulations and experimental data are presented.

1. INTRODUCTION

The resolution of incoherent imaging systems is limited by phase aberrations. They can arise from misalignments of the optics or from the atmospheric turbulence. Phase diversity (PD) is a well known technique to correct the phase aberrations[1,2]. PD requires the collection of two or more images. One of them is the conventional focal-plane image which has been degraded by the aberrations. The others are images of the same object formed by perturbing the unknown aberrations with some known aberrations. An example of phase diversity is the quadratic phase error introduced by an intentional defocusing. Gonsalves et al. [1] derived an objective function for the estimation of the aberration parameters. Nonlinear optimization has been applied to this objective function. When the aberration estimates are found, an estimate of the optical transfer function (OTF) can be constructed and the object can be restored by using a Wiener filtering.

In this paper we follow a similar approach by using a new method of collecting diverse images – aperture diversity. This technique involves forming images through different shaped apertures. Incoming wavefronts are collimated and beam-split into two or more paths to ensure the wavefront in each path have the same turbulence aberrations. Images are then formed for each path using apertures with different shapes (fig.1)

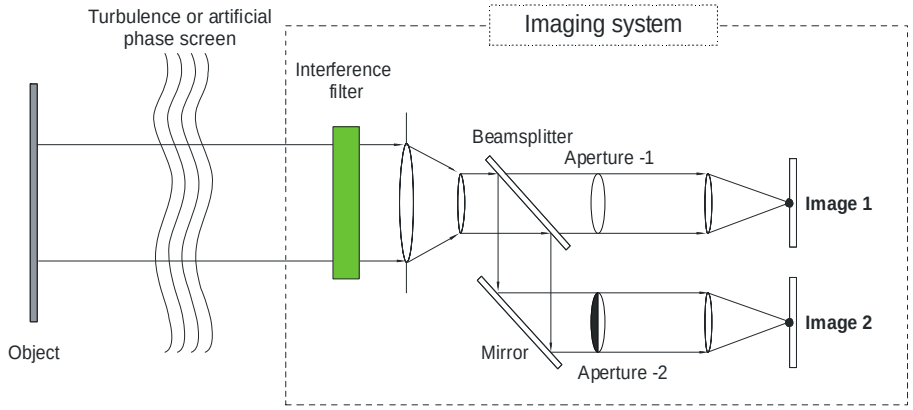

Fig. 1. Experimental setup for aperture diversity

In practice one is interested to estimate the object if the image is known. If in addition the PSF is known, the object estimation is called deconvolution. However this is a rare case. In the general case the PSF is also unknown because we don't have a clear mathematical description of the turbulence. This case is called blind deconvolution and is much more challenging. Blind deconvolution is an ill-posed inverse problem, because the contributions of the object and the PSF in forming the image cannot be separated without additional information, and solutions are thus not unique.

Use of the PSF model, Eq. (2), below, strongly constrains the estimation process by ensuring that the PSF is positive, band-limited, and physically meaningful. The problem may be further constrained by incorporating additional information through multiframe and multichannel methods. Multiframe blind deconvolution [2] assumes a common object, *o(x),* across a time sequence of images, $i_n(y)$, $n = 1...N$. In multichannel blind deconvolution, images of the same object are collected through multiple imaging channels with known intra-channel differences [1,2].

In phase diversity, two or more channels, with known phase differences, image a common object simultaneously.
An alternative to defocus for creating phase diversity is to acquire simultaneous images at two or more different wavelengths. Gonsalves and Chidlaw [3] were the first to suggest using wavelength-diverse imagery for phase retrieval, and Gonsalves [2] subsequently introduced the term "wavelength diversity". A promising wavelength diversity method was also reported by Ingelby et al [4]

2. APERTURE DIVERSITY ALGORITHM

Incoherent isoplanatic imaging is approximated by the following convolution:

$$i(x,y) = \int\int o(p,q)h(x-p, y-q)\, dp\, dq \tag{1}$$

where *i(x,y)* is the image, *o(p,q)* is the object intensity distribution, *h(x,y)* is the point spread function *PSF*.
The *PSF* of an aberrated system is given by:

$$h(x,y) = \left| \int\int GPF(u,v) e^{-i\frac{2\pi}{\lambda z_i}(ux+vy)}\, du\, dv \right|^2 \tag{2}$$

Aberrations are accounted for with a complex pupil function, called the generalized pupil function, *GPF*:

$$GPF(u,v) = P(u,v) e^{i\frac{2\pi}{\lambda} w(u,v)} \tag{3}$$

where *w(u,v)* is the cumulative optical path length error across the pupil for the optical system considered as a whole, λ is the effective wavelength and z_i is the distance from the pupil plane to the image plane.
We consider a system with M distinct channels, capable of simultaneously imaging the same scene through different apertures, $m = 1...M$. We define a frame as the set of M images captured by such a system at a given instant in time. We proceed to acquire a time sequence of N frames, indexed by $n = 1...N$. We thus have $M \times N$ images.
We define the pupil path-length errors [5], $W_n(u)$, which are common across all M channels of a single frame for an achromatic optical system. The pupil phases are then given by

$$\Phi_{mn}(u) = \frac{2\pi}{\lambda} W_n(u), \quad m = 1 \ldots M, \quad n = 1 \ldots N \tag{4}$$

We expand $W_n(u)$ in a convenient basis, such as the Zernike polynomials, so that

$$W_n(u) = \sum_k a_{kn} Z_k(u) \tag{5}$$

where a_{kn} is the weight for the k^{th} Zernike polynomial, Z_k, as ordered by Noll [6], in the n^{th} frame.
We define the discretized Fourier domain error in the m^{th} channel as

$$E_m = \sum_{n=1}^{N} \sum_{r,t} \left| I_{mn}(r,t) - S_{mn}(r,t) O_m(r,t) \right|^2 \tag{6}$$

where r, t are the spatial frequency coordinates and upper-case variables indicate the Fourier transform of lower-case (spatial domain) variables. Thus, I_{mn} is the spectrum of the image, i_{mn}, collected through the m^{th} aperture in the n^{th} frame. Similarly, S_{mn} is the spectrum of the corresponding PSF, s_{mn}, and is equivalent to an un-normalized optical transfer function [5]. Finally, O_m is the spectrum of the object intensity, o_m. Setting the derivative of E_m with respect to O_m equal to zero, assuming a common object across channels and solving for O_m, results in the inverse Wiener filter estimate of the object spectrum:

$$O = \frac{\sum_{m=1}^{M}\sum_{n=1}^{N} S_{mn}^{*} I_{mn}}{\sum_{m=1}^{M}\sum_{n=1}^{N} \left|S_{mn}\right|^2 + \gamma} \tag{7}$$

where * indicates complex conjugation. The γ term in the denominator results in greater stability in the object spectrum estimate by reducing noise amplification effects when S_{mn} is near zero [7].

Substituting Eq. (7) into Eq. (6) results in an error metric E_m for each channel m, with no explicit dependence on the object. The error is thus a function solely of the set of Zernike weights, a_{kn}, and is given by:

$$err = \sum_{r,t} \left(\sum_{m=1}^{M}\sum_{n=1}^{N} \left|I_{mn}\right|^2 - \frac{\sum_{m=1}^{M} \left| \sum_{n=1}^{N} S_{mn}^{*} I_{mn} \right|^2}{\sum_{m=1}^{M}\sum_{n=1}^{N} \left|S_{mn}\right|^2} \right) \tag{8}$$

This allows us to search for the Zernike weights that minimize this metric, and subsequently produce the optimum object estimate once these weights are found. We seek an estimate of the set of Zernike coefficients, a_{kn} that simultaneously minimizes the error function.

3. SIMULATION

The wavelength λ in our case is fixed to 550nm and corresponds to the interference filter we used in experiments. In our simulations we use different sets of apertures. The first set used consisted of only two apertures – the first being unobscured, the second having a central circular obscuration. The second set included in addition to these a third aperture – having the same area as the aforementioned central obscuration (Fig.2). In the latter case simulations showed better results because of the increased diversity. Another possibility is to have apertures in the shape of circular sectors. They can be 2, 3 or more. Figure 3 shows the 3 sectors case. The full unobscured aperture is also taken into account.

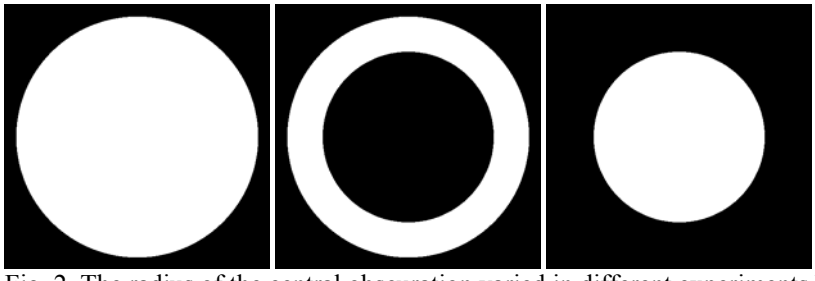

Fig. 2 The radius of the central obscuration varied in different experiments but typical values were between 0.4 and 0.7 of the full aperture (0.16÷0.5 from the total area)

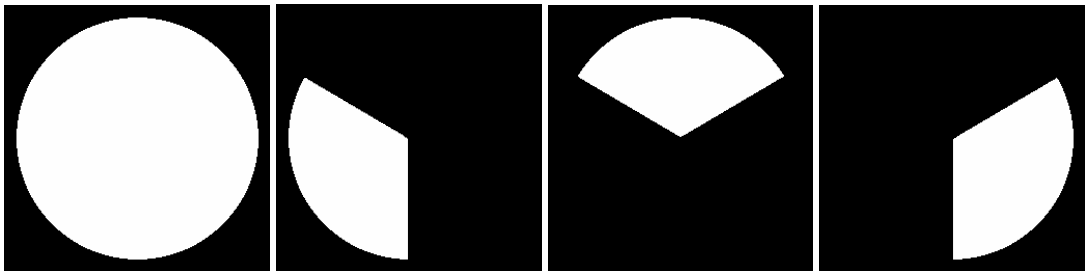

Fig. 3 Sector shaped apertures (120° each sector)

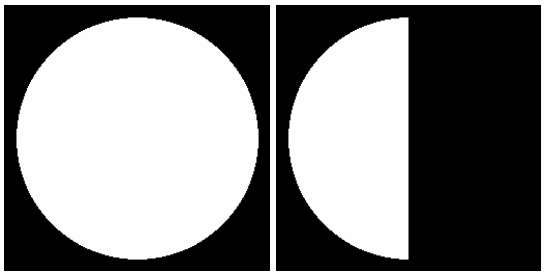

Fig.4 Sector shaped apertures (180° each sector)

Blurred images are simulated following the Kolmogorov model of atmospheric turbulence by using a method described by Roddier [8]. The goal of Roddier's method is to construct the phase screen as a functional expansion of Zernike polynomials. For each frameset an independent phase screen is constructed. The pupil phase is calculated for each of the channels and a simulated image is produced for each channel. Different magnitudes of the turbulence can be simulated. The weight estimates are then used to construct object intensity estimates using a Wiener filter — Formula (7). The object estimates are compared visually and quantitatively (by a 2D cross-correlation) to the initial undisturbed object and the blurred input images. Basically the cross-correlation of two signals provides a measure of their similarity. The discrete, normalized two-dimensional shift- and scale-invariant cross-correlation at lag (x,y), R(x,y), of two matrices A and B is given by: [9]

$$R_{\max} = \max\left\{ \frac{\sum_{\alpha=1}^{N}\sum_{\beta=1}^{N}\left[A(\alpha,\beta)-\overline{A}\right]\left[B(\alpha+x,\beta+y)-\overline{B}\right]}{\sqrt{\sum_{\alpha=1}^{N}\sum_{\beta=1}^{N}A^2(\alpha,\beta)}\sqrt{\sum_{\alpha=1}^{N}\sum_{\beta=1}^{N}B^2(\alpha,\beta)}} \right\}, \qquad (9)$$

where (x,y) span –N…N. Overbars indicate the mean of the respective quantities. An attractive feature of this metric is that the value of R_{max} is unity when the images, A and B, are identical.

3.1. SIMULATION 1

Our usual input images are 64 × 64 pixels. Typical deconvolution time for 2 channels 3 frames is 5 minutes on a Core 2 Duo E6600 processor by using MATLAB® software. The undisturbed image of a satellite is shown (Fig. 5, right). Fig. 5 shows the raw images and the result of the deconvolution by using the first two apertures of figure 2. The improvement in the object estimate in comparison to the input data is visually clear. By eye the object estimate and the original undisturbed image are indistinguishable. The quantitative estimation by the cross-correlation formula (10) is shown in Table 1.

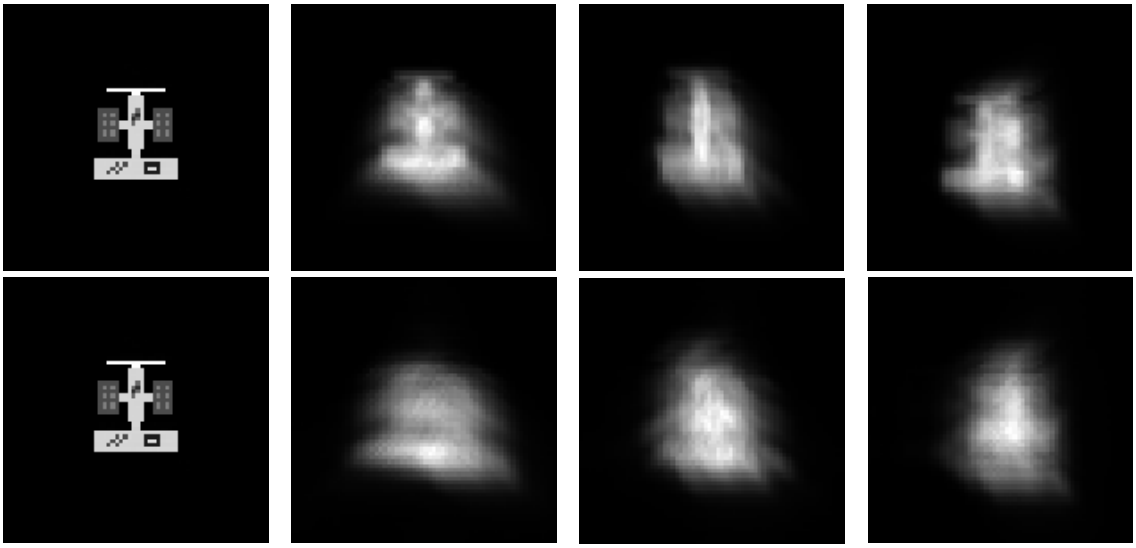

Fig. 5. Two frames, two channels (in rows). The right two columns – blurred images. Left-up – the object estimate according to formula 7, left-down: the undisturbed object.

Table 1. The correlation of the input data and the estimated objects to the original, undisturbed image. The gain is the difference between the correlation of the estimate and the highest correlation of the blurred images.

Cross correlation	Frame 1	Frame 2	Frame 3	Estimate	Gain
Channel 1	0.696	0.714	0.676	0.998	0.284
Channel 2	0.627	0.661	0.637		0.337

A combination of two minimizing algorithms is applied to the error function in order to obtain the set of Zernike weight estimates. First we started with a genetic algorithm (GA) only. It has the advantage to be able to escape local minima. However we noticed that after a certain number of iterations the GA reaches saturation and further iterations do not add much gain. At that point of saturation we switch to simplex algorithm. As a result a sharp gain is observed (fig.6). Since the simplex also saturates, even more beneficial is to switch further a few times between the genetic and the simplex algorithms.

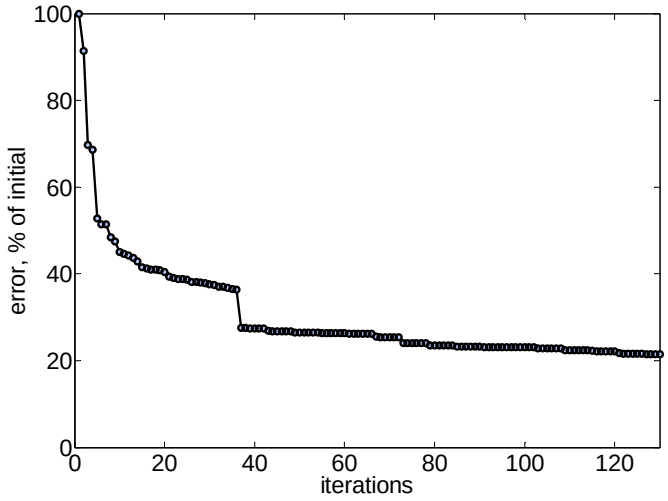

Fig. 6. Error vs iterations. Alternating the algorithms

3.2. SIMULATION 2

We hypothesize that the sector shaped apertures also bears potential since the diversity introduced by such channels can be considerable. For example, on Fig. 7, the Optical Transfer Functions of the 4 channels of 120° sectors are shown. One can see that their shapes a quite different.

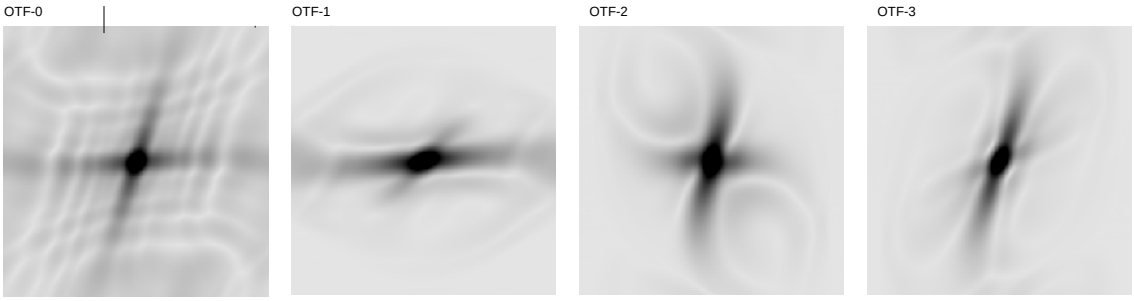

Fig. 7. Example of OTFs for the apertures shown on fig. 3

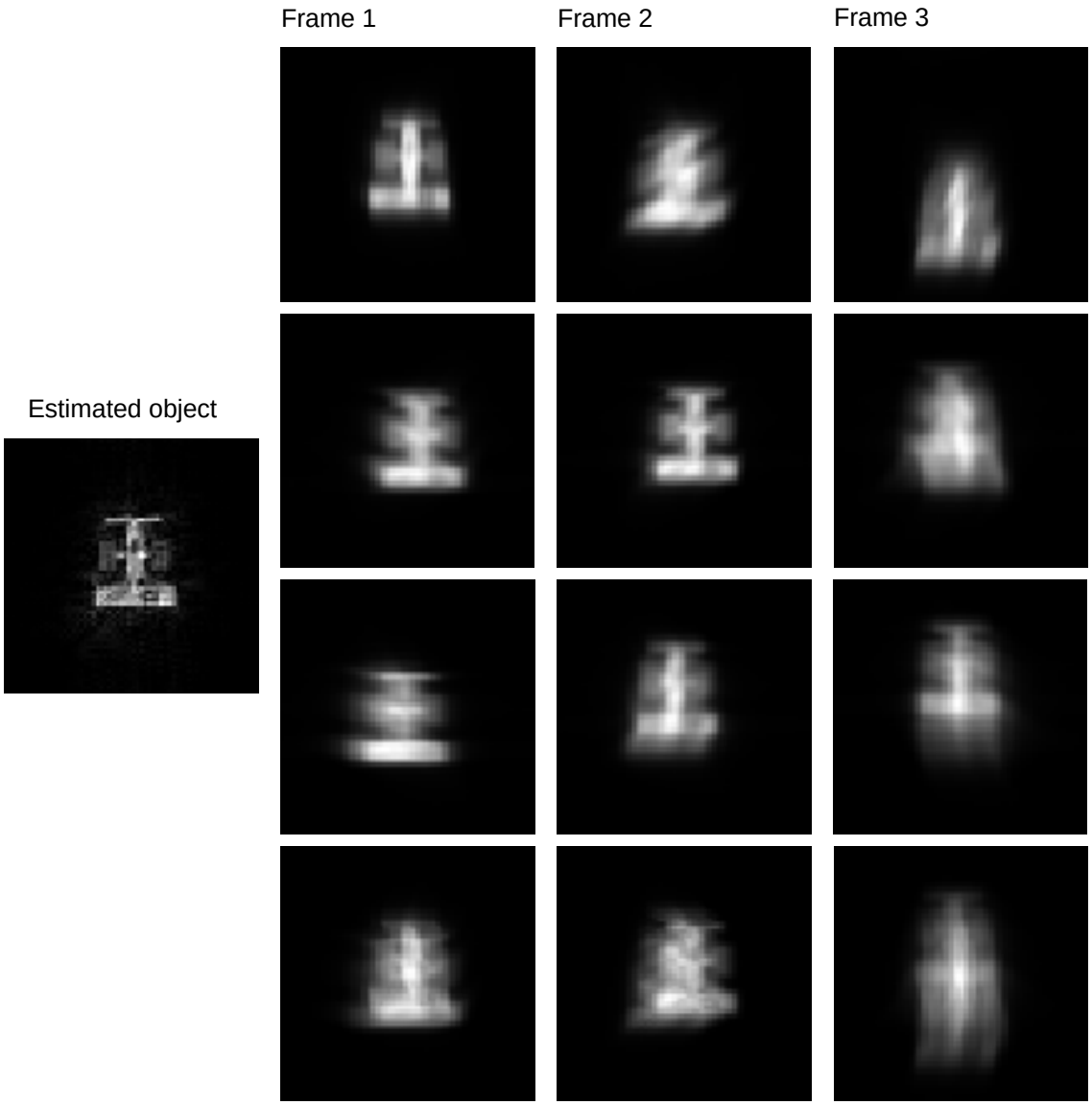

Fig. 8. Four channels (3×120° sectors + full aperture), three frames. The deconvoluted object estimate is in the left

A deconvolution result after using the 4 channels of 120° sectors is shown on Fig. 8. The object estimate is not perfect, it is still blurred but nevertheless some small details are clearly visible, while on the blurred images there are only barely visible hints of them. The quantitative (cross-correlation) results are shown in Table 2.

Table. 2. Four channels (3×120° sectors + full aperture), three frames. Cross-correlation data.

Frame	Channel 0	Channel 1	Channel 2	Channel 3
1	0.744	0.813	0.783	0.786
2	0.729	0.737	0.821	0.766
3	0.658	0.739	0.652	0.709
Estimate	0.918	0.918	0.918	0.918
Gain	0.174	0.105	0.098	0.132

We did not investigate the role of the aperture shape with the same image and same extent of blur. This problem deserves further systematic investigation.

4. EXPERIMENTAL RESULTS

In this section we present our experimental results with real images. The apertures used in the two channel experimental setup (shown in Fig.1) are shown in Fig. 4. As an object a part of the 1951 USAF Resolution Target was used. Before entering the imaging system the light passes through an interference filter, with a peak of the transmittance at 550 nm and HWHM = 5nm. The semitransparent mirror is chosen to split the light in a ratio of 1:2. Beam 1 (the upper in Fig.1) passes through a circular aperture, while the beam 2 (the stronger one) passes through a semi-circular aperture. There half of its intensity is lost so the two beams form two images of approximately the same intensity on the CCD detector. Having both images of same intensity provides better utilization of the dynamic range of the camera. After each shot, the phase screen is shifted so that the next frame is taken through a different "turbulence". We do not account for scintilations. As can be seen from Fig. 9 our algorithm showed promising results. Figure 9 shows the object estimate (left) and 3 frames of blurred data. The object estimate has a better contrast than any single input image alone. There is still some ghosting between the lines, but the overall quality is obviously improved, the lines are sharper and clearly resolved.

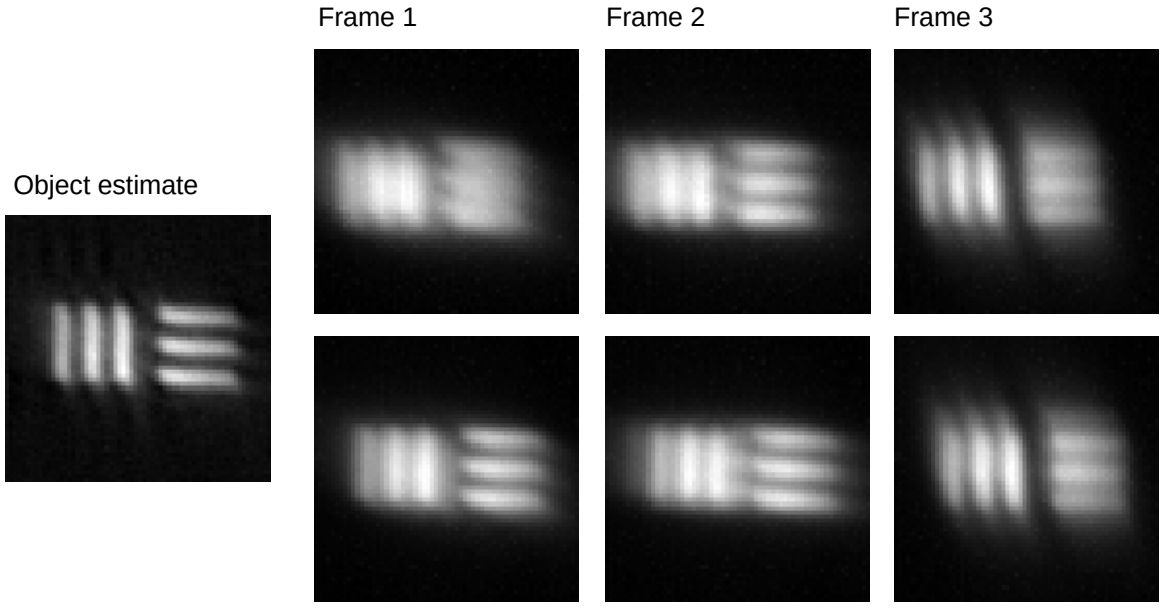

Fig. 9. Experimental results, 2 channels (the shape of the apertures is shown in Fig.4), 3 frames. Left – the estimated objects, right – the input data.

Conclusion

Aperture diversity as a method of introducing phase diversity in images is proposed. Different shaped apertures are investigated through simulations. Incoming wavefronts are collimated and split into two or more paths. In each path an aperture of different shape confines the beam. The transfer functions for each path are different (because of the different generalized pupil function) but related, thus giving a strong constraint for minimization. The deconvolution results are shown for annular and sector-shaped apertures. Experimentally the case with two apertures, one semi-circle, the other full aperture is demonstrated to work. Future plans include working with precise (pure) phase screen, a better camera, improving the minimization algorithms by using gradient techniques in order to achieve faster deconvolution times.

REFERENCES

1. R.A. Gonsalves, "Phase retrieval and diversity in adaptive optics," *Opt. Eng.* **21**, 829-832 (1982).
2. R.G. Paxman, T.J. Schulz, and J.R. Fienup, "Joint estimation of object and aberrations by using phase diversity," *J. Opt. Soc. Am. A* **9**, 1072-1085 (1992).
3. R.A. Gonsalves and R. Chidlaw, "Wavefront sensing by phase retrieval," in *Applications of Digital Image Processing III*, A.G. Tescher, ed., Proc. SPIE **207**, 32-39 (1979).
4. H.R.Ingleby and D.R.McGaughey, "Real data results with wavelength-diverse blind deconvolution", Opt. Lett. **30** No. 5, 489-491 (2005)
5. J. W. Goodman, *Introduction to Fourier Optics*, 2nd Ed. (McGraw-Hill, New York, 1996).
6. R.J. Noll, "Zernike polynomials and atmospheric turbulence," *J. Opt. Soc. Am. A* **66**, 207-211 (1976).
7. M.G. Löfdahl, "Multi-frame blind deconvolution with linear equality constraints," in *Image Reconstruction from Incomplete Data II*, P.J. Bones, M.A. Fiddy, and R.P. Millane, eds., Proc. SPIE **4792**, 146-155 (2002).
8. Roddier, N. 1990. Atmospheric wavefront simulation and Zernike polynomials. Proceedings of SPIE Vol. 1237: Amplitude and Intensity Spatial Interferometry, J.B. Breckinridge, ed., 668-679.
9. Castleman, K. 1996. Digital Image Processing. Prentice-Hall, Englewood Cliffs.